PREDICTION OF DELAMINATION IN COMPOSITE HELICOPTER ROTOR AND AIRFRAME STRUCTURES

M. R. Wisnom, G. F. J. Hill and M. I. Jones
University of Bristol, Department of Aerospace Engineering
University Walk, Bristol, BS8 1TR, U.K.
M.Wisnom@Bristol.ac.uk

Abstract

Four types of structural element typical of composite helicopter structures were designed, manufactured and tested: T-piece pull-off elements, honeycomb sandwich panel edge closures, a tapered I beam and tapered tension elements. All the elements failed by delamination, as intended. Detailed analysis was carried out using both stress based and fracture mechanics approaches and failure predictions were correlated with experimental results. In all cases the location of failure was correctly predicted, with differences between predicted and measured failure loads of between 2% and 13%.

Introduction

Delamination is widely recognised as a major limiting factor for many composite structures. Unexpected failures in structural tests frequently occur due to low through thickness strength and the lack of validated design methods. This paper describes research to develop and validate methods of predicting delamination based on analysis and testing of a series of structural elements representative of typical features on helicopter rotor and airframe structures.

Four types of structural element were designed, manufactured and tested. The first was a T-piece pull-off element representative of a skin to web joint in a stiffened skin airframe structure. The second was a honeycomb sandwich panel edge closure element based on a helicopter floor panel design, loaded in three point bending. Thirdly a tapered I beam loaded in four point bending was designed to represent a curved flange to web connection typical of that on a curved frame. Fourthly a tapered element with dropped plies loaded in tension was designed, representative of the thickness transition at the root of a rotor blade. The elements are shown schematically in Fig. 1. They were specifically designed to fail by delamination, and all the elements did fail in this mode. Detailed experimental results were obtained for comparison with analysis results. Fatigue testing was also undertaken on the sandwich panel, T-piece and tapered tension elements.

For the first three elements, failure was due to overall interlaminar stresses, and a finite element stress analysis approach was used to predict delamination. This is based on the Weibull statistical approach which is able to take account of the size effect whereby the strength decreases with increasing stressed volume. It uses an effective stress in the matrix, and accounts for in-plane as well as interlaminar stresses, thermal residual stresses and the effect of hydrostatic stress. For the tapered tension element very high stresses arise at the discontinuities where plies are dropped, which means that stress based failure criteria are unsatisfactory. A fracture mechanics approach based on energy release rates was therefore used to predict failure.

Design And Manufacture Of Structural Elements

The first element was a T-piece pull-off specimen representative of a skin to web joint in a stiffened skin airframe structure. The specimen was made from a precured skin and two cocured angle pieces all of layup $(90_2/+45/-45)_{2s}$, giving a total thickness of about 4 mm. 0° material (i.e. perpendicular to the plane of the T) was used for the fillet in the middle of the specimen, carefully shaped to fill the triangular region without any voidage. The baseline case used 5 mm radius tooling. Following a parametric study with the finite element model, a second improved variant was manufactured using 10 mm radius tooling.

The second element consisted of strips of a honeycomb sandwich panel based on the design of a helicopter floor panel. The edge closure is susceptible to delamination due to shear and bending loads where the panel reduces to a monolithic plate at the edge. Two Z-section edge pieces and the top skin were cured first. The panel was then assembled by bonding these together and incorporating an aluminium honeycomb core and the lower skin in a second cure. The top and bottom skin layups were (0/90/0/90/0) and (0/90/0), where the 0° direction

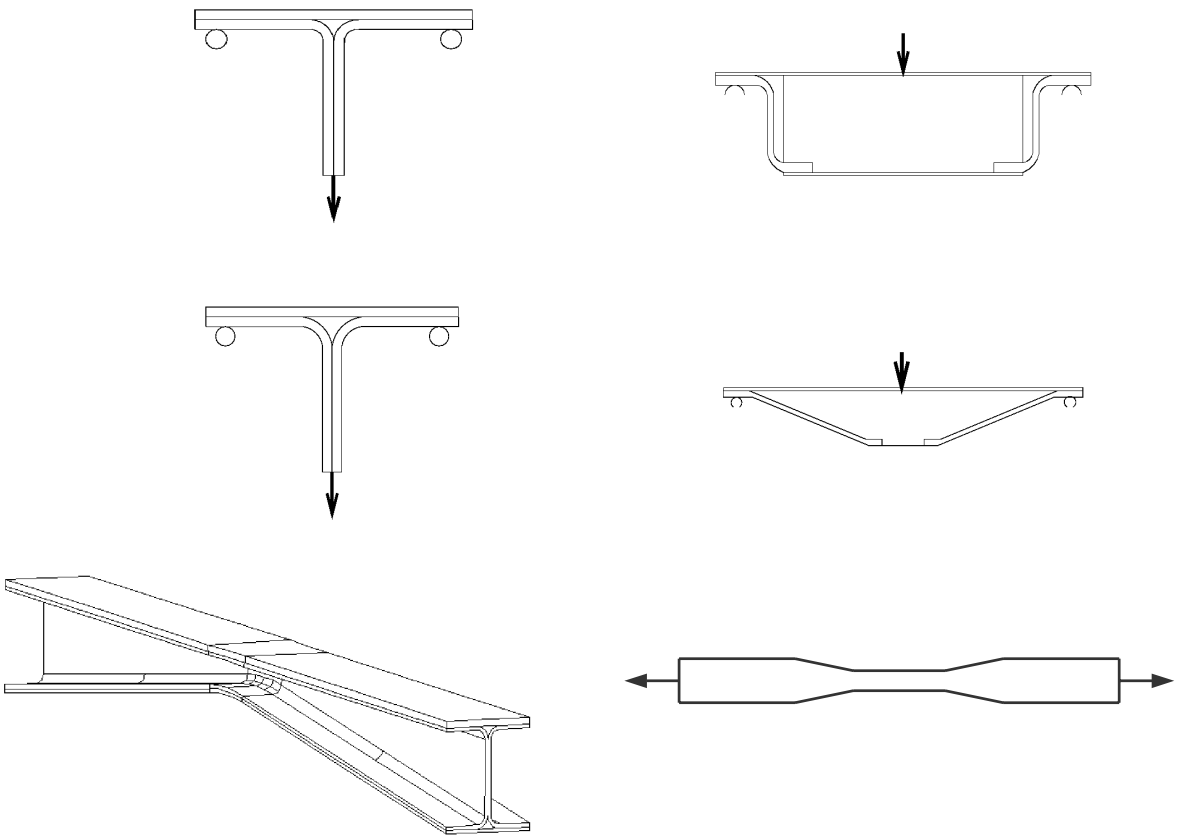

Fig. 1 Schematic of Structural Elements Studied

is across the panel. The edge pieces had a $(0/90_2/\pm45/90_2/\pm45/90)_s$ layup, with the 90° plies only in the flanges. Finite element parametric studies showed that the strength of the edge element could be greatly improved by angling the edge closures, and so a second type of element was manufactured with the honeycomb cut off at 30° to the top skin rather than 90°.

The third element was a tapered beam with a straight compression flange, and the tension flanges at an angle, with a curved section in the centre, as shown in Fig. 1. This was designed to fail due to the through thickness stresses induced by the curvature in both directions where the tension flange meets the web. The beam was 80 mm wide, with a depth of 67 mm at the ends reducing to 27 mm in the centre. The bottom flange had a central curved region about 50 mm wide with a radius of 200 mm between the two straight sections. The web and base of the flanges was formed from two back to back C-sections, each with a $(90_2/\pm45)_{2s}$ layup. Precured 0° flanges were incorporated and cobonded to the web, with additional 0° material to fill in the triangular fillet regions. The bottom flange was 16 plies thick, and the top flange was 32 plies to avoid buckling. The limited extent of the central curved section made it possible to produce high quality beams whilst avoiding wrinkling due to changes in the angle of the vertical fibres in the web.

The fourth type was a 6 mm thick 0/±45 layup tension element tapered down from both ends to a central 2 mm thick unidirectional section by dropping off plies symmetrically about the centreline. The thickness ratio is typical of that at the root of a rotor blade. The ±45° plies were dropped closest to the thin end, starting at the centre, with 0° plies dropped at the outside closest to the thick end, as shown schematically in Fig. 2. All plies were dropped in pairs, separated by continuous plies except at the start of the taper, where there is a double pair of ±45° plies dropped at the midplane. The layup in the thick section is $[(0/\underline{0}_2)_2/(0/\underline{\pm45})_6]_s$ where the underscore indicates the dropped plies. The spacing between pairs of dropped plies was 4 mm, giving a tapered section 28 mm long with an

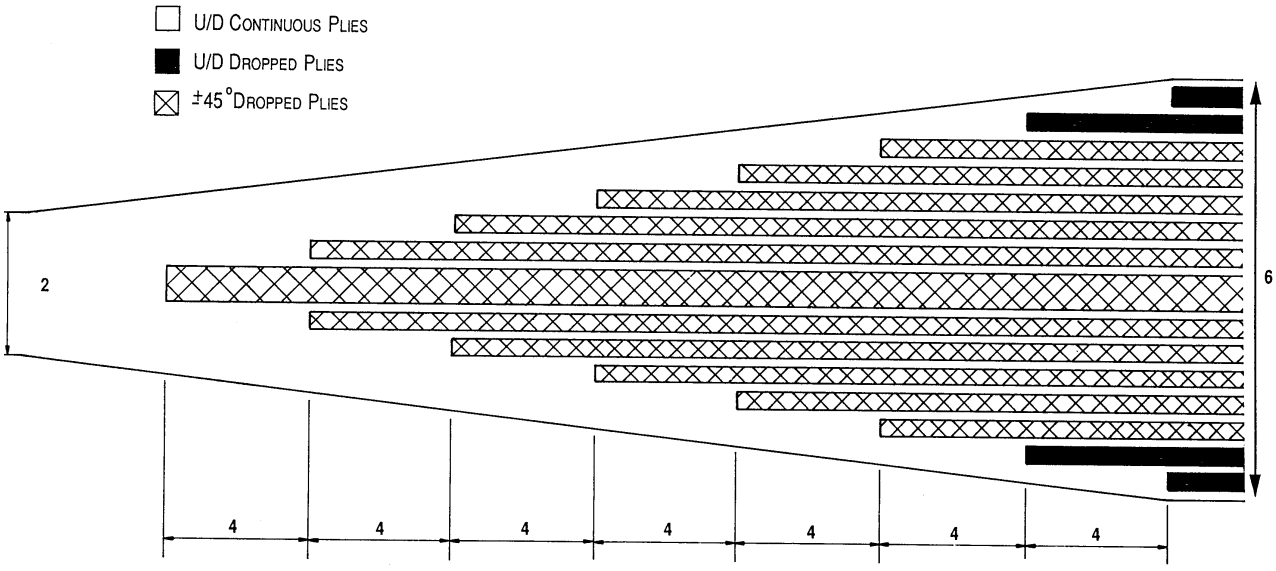

Fig. 2 Schematic of layup of baseline tapered tension specimen (dimensions in mm)

angle of about 4° on either side of the centre. The tapered plate was laid up using the ply in-fill technique whereby an equivalent tapered section is built up on the other side of the release cloth. This allowed good quality specimens to be made without the need for special tooling.

The analysis indicated that the strength of the element could be improved by dropping off the 0° plies singly. It was therefore redesigned to maximise strength, but with the same number and orientation of plies in the thick and thin sections. The layup is shown schematically in Fig. 3. Plies were again dropped symmetrically about the centreline, but now with the 0° plies dropped closest to the thin end, and then the ±45° plies. The ±45° plies were dropped in single pairs except for one double pair at the centre. Calculations suggested that failure was likely to occur by fibre breakage at the first dropped ply from the thin end. In order to maximise fibre strength, plies closest to the thin end were dropped from the outside, with a single overlaid continuous ply. This meant that the middle 14 plies were straight, whereas if plies near the thin end had been dropped further inside the specimen, more plies would have been kinked. The layup in the thick section is $[0/\underline{\pm 45}/\underline{0}/\underline{\pm 45}/(0/\underline{0})_3/(0/\underline{\pm 45})_4]_s$. A spacing of 1 mm was used between the plies dropped singly, and 2 mm between those dropped in pairs, producing a tapered section about 14 mm long with an angle of about 8° on either side of the centre.

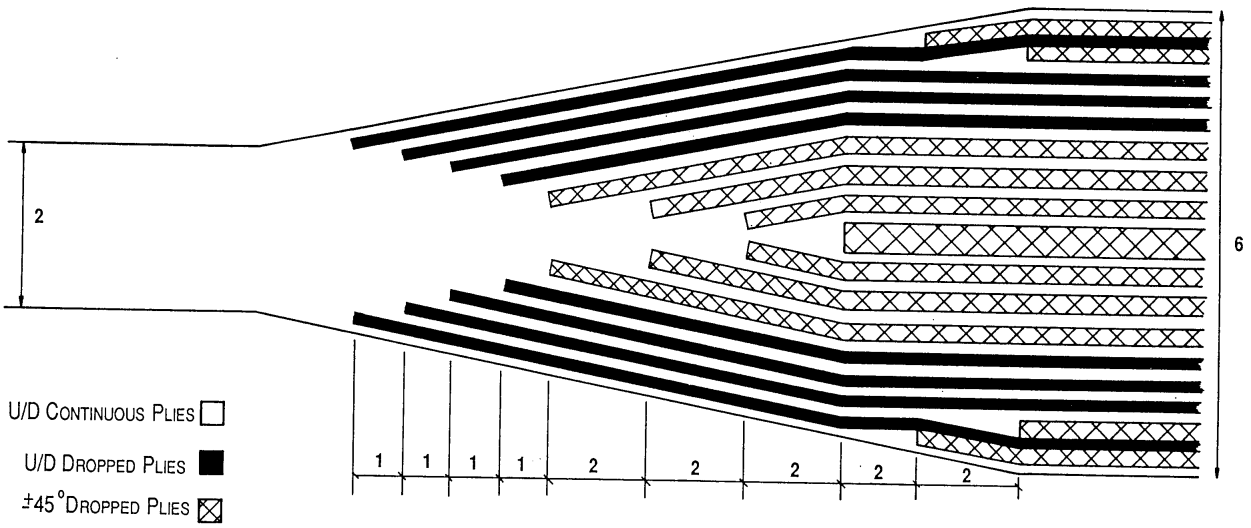

Fig. 3 Schematic of layup of redesigned tapered tension specimen (dimensions in mm)

All elements were made from Hexcel high strength carbon fibre/913 epoxy prepreg with a ply thickness of .125 mm. The first three types used HTA fibres, and the fourth used XAS. Specimens were manufactured very carefully to match the intended geometry as closely as possible and avoid introducing defects. This is essential in order to have a valid comparison between analysis and test. The separate issue of differences arising out of the manufacturing process was addressed with the sandwich panel elements by using two different manufacturing methods for the 30° element, and by carrying out finite element analysis to assess the effect of geometry variations on stress distributions.

Analysis Approach

Initial analysis indicated that in the first three cases failure was expected due to the overall state of through thickness stress. A stress based approach could therefore be used to predict failure. The tapered element had strong stress singularities at the ends of the dropped plies. These produce very high local stresses which increase as the mesh is refined. In this situation stress based approaches to failure produce mesh dependent results and so a fracture mechanics approach was adopted.

Stress Based Approach

Previous research has shown that interlaminar strength reduces with increasing specimen size [1], and so it is necessary to take account of the stressed volume to make accurate predictions of failure. This can be done using Weibull statistical strength theory. The probability of survival, P(s) of a volume V subject to a stress σ is:

$$P(s) = \exp[-V(\sigma/\sigma_o)^m] \qquad (1)$$

Where σ_o is the characteristic strength, which is a reference value for unit volume of material, and m is the Weibull modulus. This is a measure of material variability, with low values of m corresponding to high variability and hence a large size effect. These parameters can be established by testing specimens of different sizes.

Equation (1) can be generalised to the situation where the stress varies by integrating over the volume to determine the probability of survival:

$$P(s) = \exp[-\int (\sigma/\sigma_o)^m dV] \qquad (2)$$

For a unidirectional material subject to a simple uniaxial stress field this approach is reasonably straightforward, but in the present cases we need to consider 3-D geometry with several components of stress. Also we have layups with different fibre orientations, with in-plane and thermal residual stresses which may contribute to failure. A new approach was developed in order to be able to deal with all these factors [2].

Through thickness failure is driven primarily by tensile stresses in the matrix and so the method adopted was based on determining an effective matrix stress to use in conjunction with the Weibull approach. The full ply-level stress tensor was first evaluated, including the effect of thermal residual stresses. The matrix stress in the fibre direction was calculated by factoring down the composite stress by the ratio of matrix to composite modulus. For the other components the effective matrix stress was taken as being the same as the composite stress, since in each case the stresses have to pass through the matrix. The effective matrix principal stresses σ_1, σ_2, σ_3 were then calculated, and finally converted to a single equivalent value σ_e based on the Raghava equivalent stress:

$$(\sigma_1-\sigma_2)^2+(\sigma_2-\sigma_3)^2+(\sigma_3-\sigma_1)^2+0.6\sigma_e(\sigma_1+\sigma_2+\sigma_3)=2.6\sigma_e^2 \qquad (3)$$

This takes account of the effect of hydrostatic stress which is important in the yield and failure of polymers. A value for the ratio of matrix compressive to tensile yield stress of 1.3 is incorporated in (3), based on typical data for epoxy resins.

The procedure was followed on an element by element basis as a post processing operation, and the resulting stresses integrated over the volume to produce a Weibull equivalent stress $\bar{\sigma}$. This is defined as the constant stress acting on unit volume of material giving the same probability of failure as the actual stress distribution on the component of interest.

$$\bar{\sigma} = [\sum_{i=1}^{n} V_i \, \sigma_{ei}^{\,m}]^{1/m} \qquad (4)$$

where V_i is the volume of element i, σ_{ei} is the equivalent matrix stress at the centroid and n is the number of elements in the model.

Curved unidirectional beams were tested in bending to determine the interlaminar tensile strength of HTA/913. Three different sizes were tested with 16, 32 and 64 plies, and all dimensions scaled. A strong size effect was seen, as expected, with maximum interlaminar tensile stresses of 111, 103 and 88 MPa in the small, medium and large specimens [3]. A value of m of 17.7 was determined from the magnitude of the size effect. 3-D finite element analysis was applied to the specimens with the procedure described above to calculate the Weibull equivalent stress at unit volume, giving a value of 132 MPa.

The applicability of the approach to other layups was checked by performing similar tests on a curved beam with $(0_2/\pm45)_{4s}$ layup, and showing that the strength could be predicted based on the Weibull parameters from the unidirectional tests.

3-D finite element analysis was undertaken of each of the structural elements. 2-D plane strain analyses were also carried out for the T-piece and sandwich panel elements. These gave similar results, justifying the use of 2-D analysis for failure predictions. The method described above was applied to the three types of structural element, with the Weibull parameters obtained from the curved beam bending tests. Results are summarized in Table 1.

Fracture Mechanics Approach

It has been found that the dominant failure mechanism for tapered specimens with dropped plies is delamination initiating above and below the ends of the terminating plies, and propagating into the thick section along the interface between continuous and discontinuous plies [4]. The results indicate that the most important parameter affecting failure is the energy release rate associated with the terminating plies.

Delamination can be predicted based on calculating the strain energy release rate from a simple equation, and comparing it with a value for the fracture energy. This method has been found to give good predictions of delamination for simple unidirectional tapered sections [5].

Assuming a particular delamination location, the energy release rate G can be calculated in terms of the applied load per unit width P by:

$$G = P\,(K_o - K^*)/4K_oK^* \qquad (5)$$

where K_o is the in-plane stiffness of the section before delamination, defined as the axial force per unit width for unit applied axial strain, and K^* is the stiffness after delamination assuming that the delaminated plies carry no load and that the remaining blocks of material are unconnected [8].

Where there are only 0° plies, K is simply the product of the fibre direction modulus and the thickness. Where ±45° plies contribute to the stiffness, K can be calculated by laminated plate theory. The delamination is driven primarily by shear, with some through thickness compressive stresses present, so the mode II fracture energy G_{IIc} is used to compare with G to predict failure. Results are summarized in Table 1.

Table 1: Correlation of Predicted Strengths with Experimental Results

Structural Element	Test Failure Load (kN)	Predicted Failure Load (kN)	Difference
T-piece element 1, 5 mm radius	2.26	2.04	-10%
T-piece element 2, 10 mm radius	3.86	3.36	-13%
Sandwich element 1, 90° precured	2.33	2.38	+2%
Sandwich element 2, 30° precured	6.32	5.88	-7%
Sandwich element 2, 30° cocured	6.28	6.84	+9%
Tapered I-beam specimen 1	22.4	25.3	+13%
Tapered I-beam specimen 2	17.1	18.4	+8%
Tension element, 4° taper	37.3	35.5	-5%
Tension element, 8° taper	44.1	40.7	-8%

T-Piece Elements

T-piece specimens 20 mm wide were gripped by the web in the test machine and pulled against two rollers 80 mm apart supporting the skin. Failure occurred suddenly, initiating in the fillet region. Six specimens were tested and the results were very repeatable. Despite the care in manufacture, two other specimens were found to have visible voids in the fillet region. These had strengths of about half the others, showing the critical importance of manufacturing defects.

The finite element analysis showed that tensile stresses across the fillet due to bending of the skin were the main cause of failure, with some contribution from shear stresses. The 2-D half symmetric model is shown in Fig. 4 together with a typical contour plot showing the distribution of horizontal stress. The peak value occurs at the interface between the curved plies and the fill-in material, about half way around the radius. Residual thermal stresses in the fillet were also found to be significant. Interlaminar tensile stresses in the curved sections gave another possible failure mechanism, although less critical for this geometry. The predicted failure load was 10% conservative, and failures occurred where expected based on the stress distributions.

A parametric study showed that the modulus of the fill-in region had relatively little effect on the strength of the joint. Increasing the corner radius reduced stresses significantly. Changing the shape of the fillet by increasing the radius away from the skin gave a further reduction compared with a constant radius design with the same volume of material.

Based on the parametric study, an improved design with a 10 mm tool radius was made and tested. This was predicted to increase the strength by 65% whilst keeping the geometry simple. The tests gave a 71% higher failure load, validating the predictions and showing the considerable scope for improvement in strength based on a sound understanding of the stresses and failure modes. Further details of the T-piece analysis and tests are given in [6].

Sandwich Panel Edge Elements

Sandwich panel specimens 40 mm wide were tested in three point bending, with an outer span of 200 mm and a large central roller to distribute the load. Four specimens of each type were tested. The baseline 90° element delaminated in the top corner of the Z-section due to the combination of interlaminar shear and tension in the curved region.

A detail of the finite element model in this corner of the edge element is shown in Fig. 5. The geometry was based on micrographs of a sectioned specimen. Fig. 6 shows contours of the interlaminar tensile stress for a load of 50 N/mm with thermal residual stresses included. A peak stress of over 50 MPa arises due to the tension in the curved inner 0° plies. The analysis predicted the correct location of failure, at a load only 2% higher than measured.

A parametric study was undertaken to assess the effect of changes in the radius, thickness and angle of the edge closure. All of these factors

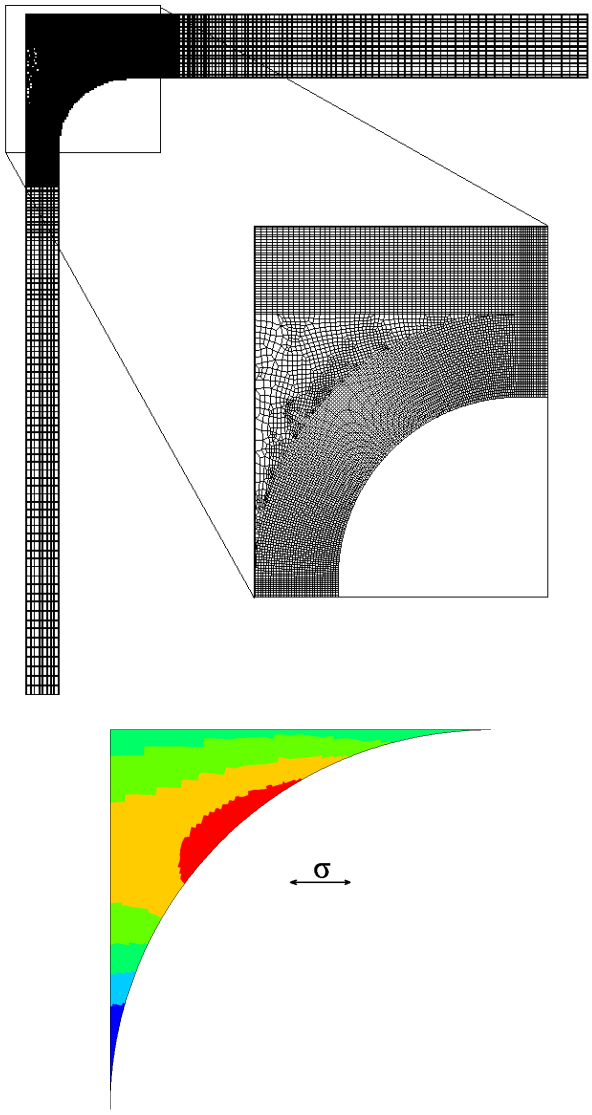

Fig. 4 T-piece finite element mesh and typical plot of horizontal stresses in fillet

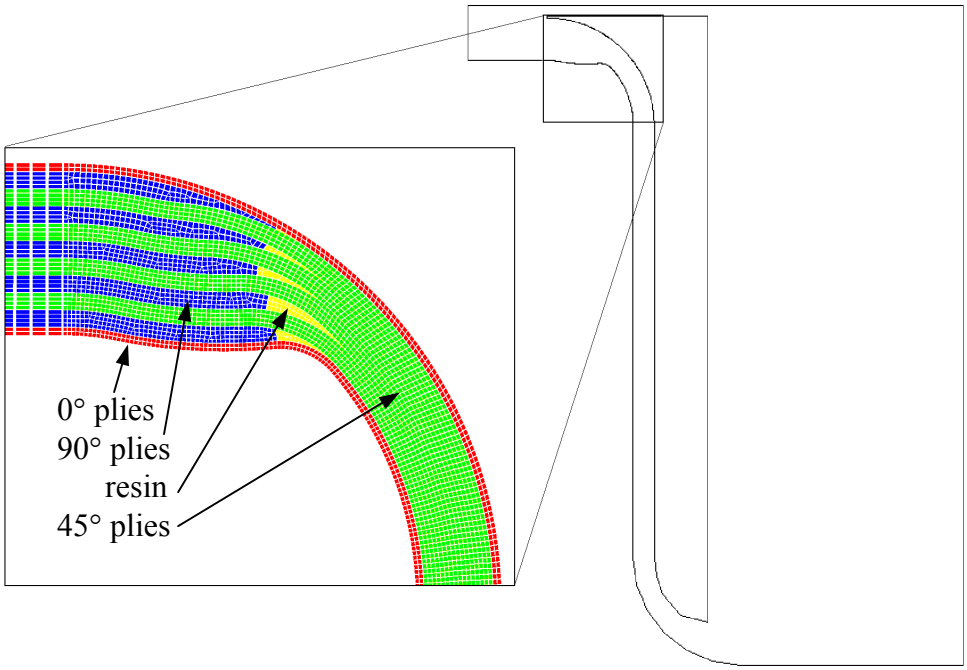

Fig. 5: Detail of finite element model of 90° sandwich panel edge element

made a significant difference to the stress distributions, but reducing the angle from 90° to 30° had the largest effect and so a second structural element with this geometry was manufactured. The closure pieces were cured and bonded to the honeycomb in one operation without any top tooling and on inspection significant differences were found from the nominal geometry. Finite element analysis showed that the detailed geometry had a significant effect on the stresses, and so the as-manufactured geometry was modelled. The strength of the 30° element was predicted to be 187% higher than the baseline 90° element. The tests showed a similar increase in failure load of 169%.

The analysis indicated even higher strengths with better controlled geometry. To investigate this and to quantify the effect of variations in the manufacturing process a second set of 30° elements was made with the edge elements precured using a metal tool. Although this improved the edge pieces, they were found not to be fully bonded to the honeycomb due to slight differences in geometry. Test results were similar to the cocured elements, and the analysis showed that this was because the lack of bonding counteracted the improvements due to the edge piece geometry local to the delamination zone.

These results validated the approach to failure prediction and demonstrated how the current design could be greatly improved. In addition they showed that variations in geometry arising in the manufacturing process have significant effects, and that these can also be predicted by finite element analysis.

Tapered I-Beam Elements

The I-beam was the largest and most complex of the elements tested, with a length of about 700 mm. It was tested in four point bending, with outer and inner spans of 600 mm and 200 mm respectively. The web was filled with epoxy resin in the vicinity of the loading rollers to avoid local failure. Further details of the design and testing are given in [7]. The beam took a considerable time to manufacture, and so only two were made. The web of the first beam was tapered due to some movement of the tooling. This was overcome in the second beam, but meant that the geometries were slightly different.

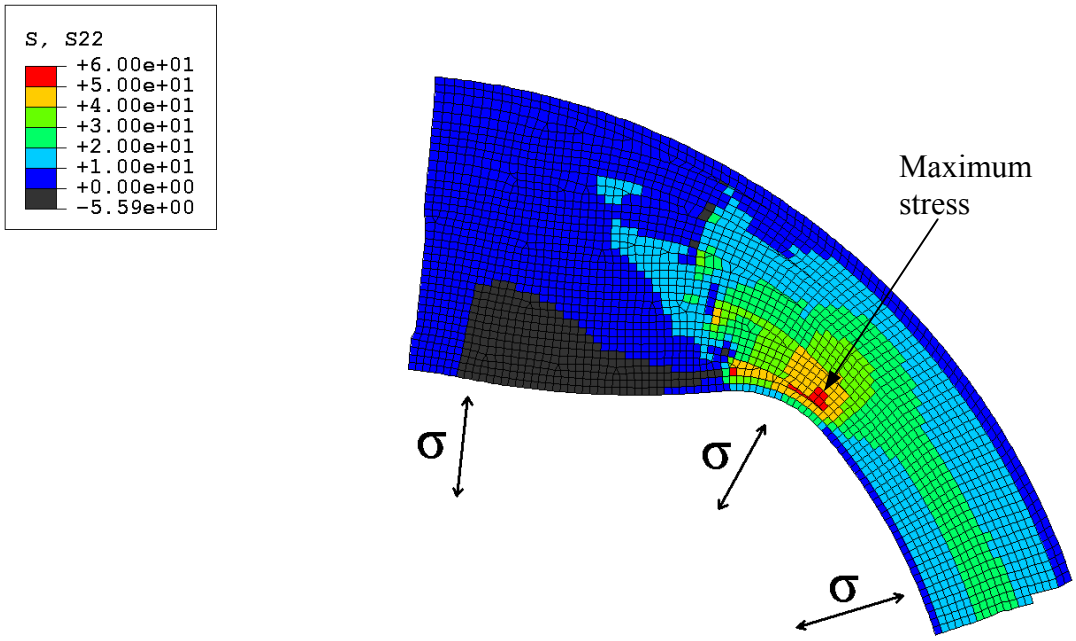

Fig. 6 Interlaminar tensile stresses in corner of 90° sandwich panel edge element

The first beam was tested to failure. Fig. 7 shows it set up in the test machine. Distinct cracks were heard starting at 22.4 kN. These were also registered from disturbances on strain gauges attached to the flanges. The beam continued to carry load until catastophic failure with the whole bottom flange detaching at 37 kN. The second beam test was stopped after the first crack at 17 kN. No damage was visible, but on sectioning the beam it was found to be delaminated in the doubly curved region at the web to flange connection in the middle of the beam.

The finite element analysis predicted failure due to a combination of interlaminar tension and shear in the curved region very close to where delamination was found. The analysis correctly predicted the lower strength of the second beam due to the differences in geometry, and the predicted failure loads for the two beams were 13% and 8% higher than the measured ones.

Tapered Tension Elements

Plates were cut into specimens 10 mm wide and four of each type were loaded in tension to failure. For the baseline 4° tapered tension element first failure occurred when the two surface plies on one side delaminated and fractured. It appeared that failure had initiated by delamination into the thick section at the forwardmost pair of 0° plies.

The redesigned specimens with the 8° taper failed at a higher load, as expected. Failure was catastrophic, with fibre failure mainly concentrated around the thin end of one of the tapers, but with no indication of prior delamination.

The energy release rates were calculated using equation (5). For the baseline specimen, delamination at the drop of 0° plies nearest the thin end is most critical. Laminated plate theory was used to calculate the stiffness of the whole section at this location before delamination. The layup here is effectively $[0_2/\underline{0_2}/(0/\underline{\pm 45})_6]_s$ because the other two pairs of 0° plies have already been dropped. After delamination the stiffness of the centre section of layup $[(0/\underline{\pm 45})_6]_s$ was calculated in the same way. The outside two pairs of continuous unidirectional plies were assumed to still carry load, but to act independently from the rest of the section with the same fibre direction strain. Their stiffness was therefore calculated separately and added to produce the total stiffness after delamination. Since the specimen is symmetric, it was assumed that the two blocks of plies on either side of the centreline delaminate simultaneously. The total strain energy release rate from equation (5) needs to be divided by two to get the value of G associated with the delamination on each side. A fracture energy of 0.82 N/mm was used, derived from delamination of simple unidirectional specimens with terminated plies [8].

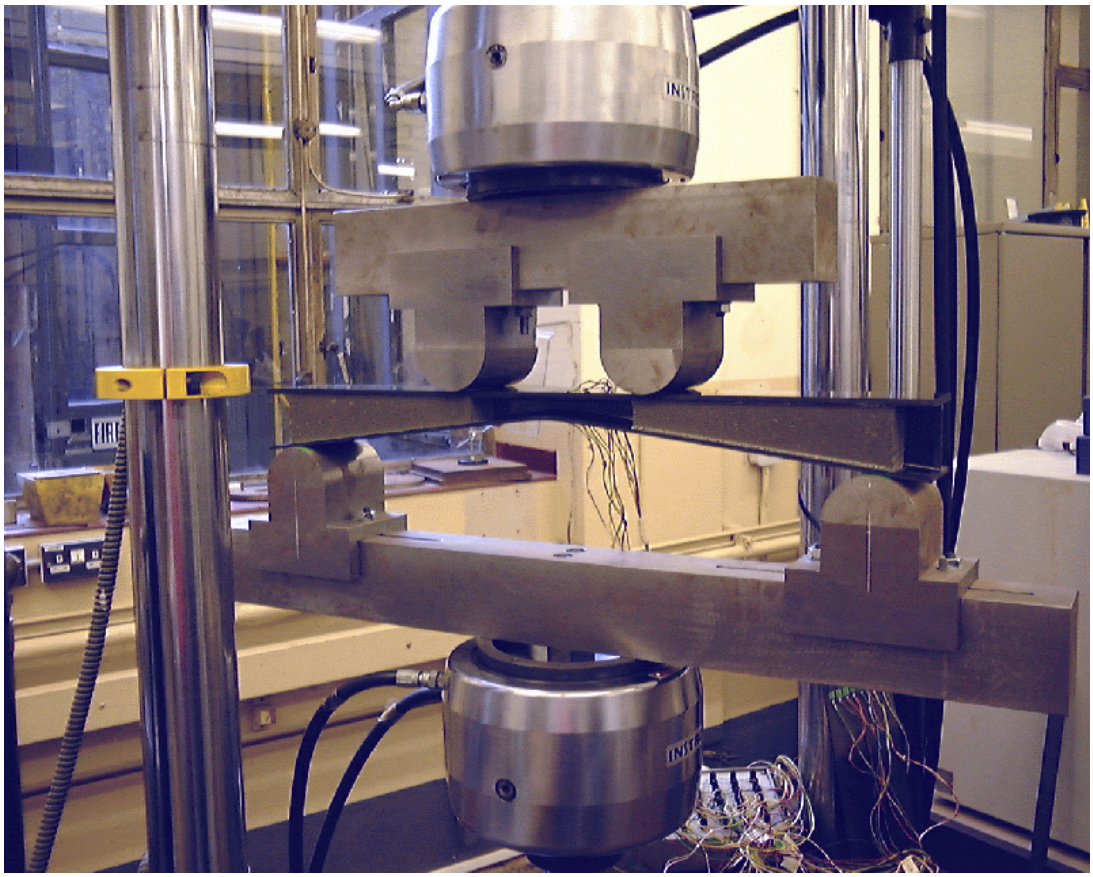

Fig. 7 Tapered I-beam four point bending test

The predicted failure load was about 5% below the measured value, as shown in Table 1. The predicted failure mode was also consistent with the observations.

For the redesigned specimen, the dropped 0° plies nearest the thin end were found to be the critical case. The predicted failure load was about 8% below the measured value. The predicted delamination stress of 2002 MPa was similar to the fibre direction tensile strength of 2105 MPa. The closeness of these values explains the catastrophic failure with fibre fracture observed in the tests.

The improvement in strength of 18% was similar to that predicted. It is widely believed that it is the taper angle that is important in determining strength. The fact that the stronger specimen had a steeper taper angle disproves this, and shows that it is the number of plies dropped together that is the critical factor.

Further details of the tapered tension element analysis and tests are given in [8].

Fatigue Tests

A set of constant amplitude fatigue tests was carried out on T-piece elements with maximum loads of 50% to 75% of the static strengths. Failure occurred suddenly, with similar location of cracks to that observed under static loading. Tests were also performed on 30° sandwich elements. The overall results were broadly in line with previous tests in terms of mean life for a given maximum load as a proportion of static strength [9]. This suggests that fatigue strength could be estimated from static element test or analysis results combined with coupon tests to characterise the fatigue performance.

Fatigue tests on the tapered tension elements showed delamination initiating at the 0° ply drops closest to the thin section, and propagating stably into the thick section. It was found that a Paris law approach based on the same energy release rate equation as used for static strength was able to predict delamination growth rates remarkably well [8].

Conclusions

A series of structural elements has been designed, manufactured and tested containing typical features seen on composite helicopter airframe and rotor structures. All the elements failed by delamination, as intended, and detailed results were obtained for comparison with analysis.

A stress based approach for predicting delamination has been presented which can be applied to components with 3-D geometry and any layup. It is based on the effective stress in the matrix, and accounts for in-plane as well as interlaminar stresses, thermal residual stresses and the effects of hydrostatic stress and stressed volume. The approach has been applied to three types of elements. In all cases the location of failure was correctly predicted, with differences between predicted and measured failure loads of between 2% and 13%.

A fracture mechanics approach has been presented based on calculating the energy release rate associated with delamination. This overcomes the problems with stress based approaches at singularities caused by discontinuities such as dropped plies. The approach worked well for the tapered tension elements, predicting failure within about 8%.

The experimental and analysis results both showed the importance of defects and variations in geometry arising in manufacture, and that their effects can be predicted by finite element analysis.

Three of the elements were redesigned based on parametric studies, and increases in strength of 71%, 169% and 18% were measured, similar to the predictions. These results further validated the analysis approaches and demonstrated the improvements in strength that can be achieved based on a sound understanding of the stress distributions and failure modes.

Acknowledgement

This work was funded by EPSRC/MoD under contracts GR/L25721 and GR/F/28687 in collaboration with GKN Westland Helicopters.

References

1. Wisnom, M.R., Size effects in the testing of fibre-composite materials, Composites Science and Technology 59:1937-1957, 1999.

2. Hill, G. F. J., The development and application of delamination prediction methods for composite structures, PhD thesis, University of Bristol Department of Aerospace Engineering, 2001.

3. Wisnom, M. .R., Jones, M. I. and Hill, G. F. J., Interlaminar Tensile Strength of Carbon Fibre-Epoxy – Specimen Size, Layup and Manufacturing Effects, Advanced Composites Letters, 4:171-177, 2001.

4. Wisnom, M.R., Prediction of Delamination in Unidirectional Glass Fibre-Epoxy with Tapered Thickness, AIAA Structures, Structural Dynamics and Materials Conference, Baltimore, U.S.A., pp 1162-1172, April 1991.

5. Wisnom, M.R., Prediction of delamination in tapered unidirectional glass fibre epoxy with dropped plies under static tension and compression, AGARD meeting on Debonding/Delamination of Composites, Patras, Greece, May 1992, AGARD CP530 pp 25/1-7.

6. Hill, G. F. J., M. R. Wisnom and M. Jones, Failure prediction of composite T-piece specimens, 5th International Conference on Deformation and Fracture of Composites, pp 169-178, London, March 1999.

7. Hill, G. F. J., M. R. Wisnom and M. Jones, The design, manufacture and test of a tapered composite I-Beam, Proc. ICCM12, Paper 980, Paris, July 1999.

8. Wisnom, M.R., Jones, M.I., and Cui, W., Failure of tapered composites under static and fatigue tension loading, AIAA Journal 33:911-918, 1995.

9. Wisnom, M. R. and Jones, M. I., Through thickness fatigue failure of fibre reinforced composites, The Aeronautical Journal 102:83-88, 1998.